Journal of Alloys and Compounds 510 (2012) 54–59

Contents lists available at ScienceDirect

Journal of Alloys and Compounds

journal homepage: www.elsevier.com/locate/jallcom

Tunable light emission and similarities with garnet structure of Ce-doped LSCAS glass for white-light devices

L.H.C. Andrade[a,*], S.M. Lima[a], M.L. Baesso[b], A. Novatski[b], J.H. Rohling[b], Y. Guyot[c], G. Boulon[c]

[a] Grupo de Espectroscopia Óptica e Fototérmica, Universidade Estadual de Mato Grosso do Sul – UEMS, C.P. 351, Dourados, MS, Brazil
[b] Grupo de Estudos de Fenômenos Fototérmicos, Departamento de Física, Universidade Estadual de Maringá, Av. Colombo 5790, 87020-900 Maringá, PR, Brazil
[c] Laboratoire de Physico-Chimie des Matériaux Luminescents, Université Claude Bernard Lyon 1, UMR 5620 CNRS, 69622 Villeurbanne, France

ARTICLE INFO

Article history:
Received 8 February 2011
Received in revised form 9 August 2011
Accepted 10 August 2011
Available online 19 August 2011

Keywords:
Ce-doped LSCAS glass
Smart white-light
Phosphors
Amorphous materials
Optical materials
Optical properties

ABSTRACT

In this paper, we report results concerning tunable light emission and color temperature in cerium-doped low-silica-calcium-alumino-silicate (LSCAS) glass for smart white-light devices. Spectroscopic results, analyzed using the CIE 1931 *x*–*y* chromatic diagram, show that this glass presents two broad emission bands centered at 475 and 540 nm, whose intensities can be tuned by the excitation wavelength. Moreover, the same emission can be achieved from a color temperature range from 3200 to 10,000 K, with a color-rendering index (CRI) of around 75% obtained by changing the optical path length of the sample. Our new phosphor LSCAS glass, which is a unique system that exhibits tunable yellow emission, combines all qualities for white-light devices.

1. Introduction

Recently, much effort has been dedicated to develop luminescent materials able to produce a new generation of white light (WL) for light sources and components used in electronic display devices [1]. White-light-emitting diodes (WLEDs) and many materials doped with luminescent ions have been studied as potential WL generators. Among those materials with luminescent ions, the most used are oxides doped with rare-earth ions like Sm^{3+}, Pr^{3+}, Tb^{3+}, Dy^{3+}, Eu^{3+} and Eu^{2+} and co-doped with Ce^{3+} ions as activators [2–7]. In particular, the Ce^{3+} ion is interesting for phosphors due to both short lifetime (about 50 ns) and a broad emission band centered between 350 and 550 nm that is associated to the allowed $5d \rightarrow 4f$ electronic transition [8]. One material that has been extensively studied is the phosphor Ce^{3+}:YAG, which presents a broad yellow luminescence when excited with sources emitting in the range between 410 and 480 nm. This system is very interesting because the radiation of the GaN-based UV-blue LED can used simultaneously for excitation and to be added to the yellow emission of the Ce^{3+}:YAG, with an appropriate intensity, yielding WL [9–11]. Although crystals are interesting for WL generation, they have some disadvantages: their production is expensive, difficult to grow and demand high Ce^{3+} concentrations (~2 at.%), leading to fast luminescence quenching. Another drawback of Ce^{3+}-doped crystals is the low color-rendering index (CRI), which is due to its very weak emission intensities in the red region [10]. There are few Ce^{3+}-doped crystals emitting in the yellow region, and, until recently, those reported in the literature exhibit a garnet structure [10–13]. For other Ce^{3+}-doped materials, the emissions are located in the UV or blue spectral regions.

In the last few years, we have focused our attention on the study of the optical properties of OH^- free rare-earth and metal-transition-doped low-silica-calcium-aluminosilicate (LSCAS) glass. This glass exhibits phonon energy of approximately 800 cm^{-1}, lower than those of silicate glasses [14]. When co-doped with Er^{3+}/Yb^{3+}, it presents high emission rates in the mid infrared, near 2.8 μm [15]. Additionally, laser emission at 1.07 and 1.37 μm were observed when this glass was doped with Nd^{3+} [16] and Yb^{3+} [17]. More recently, a long lifetime (~2.0 ms at 77 K and 170 μs at room temperature) and a broad emission band of 190 nm (4237 cm^{-1}) centered at 637 nm (15698 cm^{-1}) were found in a Ti^{3+}-doped LSCAS glass [18], which also shows high values of both gain cross section (~4.7×10^{-19} cm^2) and luminescence quantum efficiency (~70%) [19] comparable to the values for Ti^{3+}:sapphire crystals. Our most recent achievement in this host glass was to show that, when doped with cerium, it can produce smart WL combining a glass phosphor with light-emitting diodes (LEDs) at 405 nm, resulting in an emission close to ideal WL [20].

* Corresponding author. Tel.: +55 67 3902 2653; fax: +55 67 3902 2652.
E-mail address: luishca@uems.br (L.H.C. Andrade).

0925-8388/$ – see front matter © 2011 Elsevier B.V. All rights reserved.
doi:10.1016/j.jallcom.2011.08.053

In this work, we deal with results concerning the possibility of tunable emission in Ce^{3+}:LSCAS glass in two ways: by changing the excitation wavelength within the violet and blue regions or by changing the re-absorption by varying the sample thickness. A structural interpretation was proposed to explain this glass particularity, which indicates that the LSCAS glass system is able to change its color temperature in accordance to the occasion. This is very interesting for the regulation of the circadian rhythms of humans, which is a great advantage for this material when compared with crystals. This matter of circadian rhythms will be a new direction of research for commercial luminophosphors of interest for artificial lights.

2. Experimental details

2.1. Sample preparation

The glass, in wt.%, were prepared with high-purity oxides having 41.5% of Al_2O_3 (5N), 47.4% of CaO (5N), 7% of SiO_2 (5N), 2.1% of MgO (5N) and 2.0% of CeO_2 (4N). The mixture was melted under vacuum atmosphere at 1600 °C for 2 h, condition used to remove the OH^- molecules from the glass structure. This procedure revealed to be a successful route to obtain a high ratio of Ce^{3+} oxidation state in the glass. The glasses presented excellent yellow-coloration homogeneity and transparency. It is important to mention that this glass presents excellent thermomechanical properties as shown before for the undoped and rare earth doped samples [21,22]. For the measurements, the sample was optically polished until reaching a thickness around 1.5 mm.

2.2. Spectroscopic characterization

Experiments were performed through optical absorption (OA), UV–Vis optical excitation (OEx) and emission (OEm), and micro Raman spectroscopy. The emission spectra were analyzed in a CIE 1931 color diagram.

The OEx experiments were carried out using a 450 W Xe^+ lamp and a H10D Horiba-Jobin Yvon monochromator. The OEm was collected by an optical fiber and analyzed by a Triax 320 Jobin Yvon monochromator with a 600-grooves/mm grating, a 0.05 nm resolution and a Peltier cooled charge-coupled-device detector (CCD). The dependence of the emission spectra as a function of the excitation was obtained by scanning the excitation wavelengths from 200 to 450 nm with 5 nm steps and recording the optical emission for each excitation.

The Raman spectra obtained with an excitation wavelength at 632 nm (supplied by a He–Ne laser) were recorded by a LabRAM ARAMIS (Horiba–Jobin–Yvon) spectrometer with a 1800-grooves-per-mm grating with a microscopic attachment (objective X50), associated with an Edge filter to reject the Rayleigh line. The signal was collected with a cooled Andor CCD. The acquisition time integration was 60 s.

3. Results and discussion

3.1. Tunable light emission spectroscopy

Fig. 1(a) shows the optical excitation and emission spectra for the 2 wt.% CeO_2-doped LSCAS glass. The excitation spectra were developed by observing the emission at 410 and 550 nm. Two main excitation bands centered at 325 (UV) and 405 nm (violet) are observed, which are responsible for two broad emission bands centered at 475 (blue) and 540 nm (yellow), respectively. The blue emission observed under UV excitation is commonly found in many Ce^{3+}-doped materials reported in the literature, except in Ce^{3+}-doped non-garnet materials [10]. The intense and broad yellow emission is characteristic of Ce^{3+}-doped garnets crystals [10–13]. Fig. 1(b) shows the optical absorption cross section with the excitation spectra for the 570 nm emission. It can be observed that this excitation band, responsible for the broad yellow emission, fitted inside the absorption cross section spectra, does not match with the maximum of the absorption band. The maximum cross section for this band, obtained from graph is 1.44×10^{-20} cm^{-2} at 409 nm. As already presented in Fig. 1(b) of Ref. [18], despite this excitation band (absorption) be much less intense than that of the UV one, the emission in the yellow region is more intense than that in the blue, which means that its quantum efficiency is higher. The origin of these two emission bands is related to two main sites of the Ce^{3+} ion in the glass, which will be discussed later.

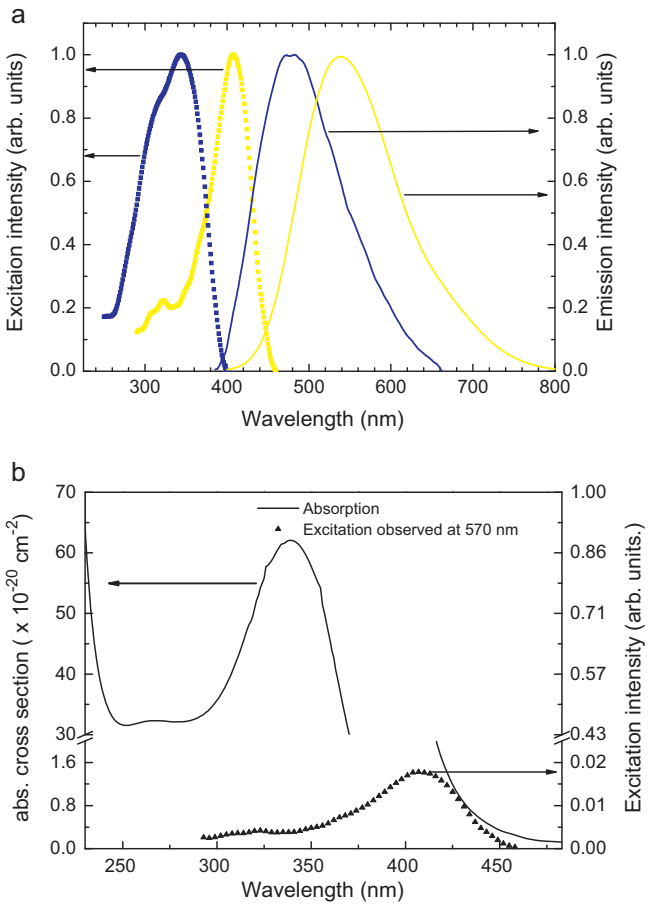

Fig. 1. (a) Optical excitation and emission of 2 wt.% CeO_2-doped LSCAS glass, monitoring the emission at 410 and 550 nm. The blue line is the emission obtained under 320-nm excitation, and the yellow line represents the emission under 405 nm excitation. (b) Absorption cross section spectra of the same glass with the excitation spectra for 570 nm emission.

It is important to note that there is a superposition of two broad excitation bands. In this case, it is possible to obtain continuously different emission bands by changing the excitation wavelength. Fig. 2 shows the CIE 1931 color diagram for different excitation wavelengths from 305 to 425 nm. The maximum peaks of the emission wavelength from 305 to 365 nm do not change significantly. From 365 to 425 nm, a 10-nm change in the excitation wavelength leads to a significant change in the CIE color coordinate, and the emission shifts from the blue to the yellow region. In addition, correlated color temperature CCT decreases from about 10,000 to 3200 K, when the excitation wavelength is increased. This displacement is also followed by a broadening of the emission band. The CIE 1976 uniform color diagram indicate that (u', v') color coordinates for 365 nm and 425 nm excitation wavelength, mentioned before, change from (0.15, 0.46) to (0.19, 0.48). The spectra shown in Fig. 1(a), obtained under 410 nm excitation (the wavelength of the maxima emission intensity), indicate a CCT of 4450 K and a (u', v') color coordinates of (0.19, 0.54). Then, the nearest distance from the Plank locus (Duv) in (u', v') color diagram is 0.058. Table 1 summarizes the emission properties of some garnet crystals that can be compared with the Ce^{3+}:LSCAS glass. As observed, the emission spectra of this glass have a similar peak position compared with those of Ce^{3+}-doped garnet structure, but shows a broader band. Moreover, the other Ce^{3+}-doped materials present their emission band in just one fixed spectral position in the UV and blue or, in the case of materials with garnet structure, in the green or yellow regions [12,23]. Taking account the emission of a LED emitting at

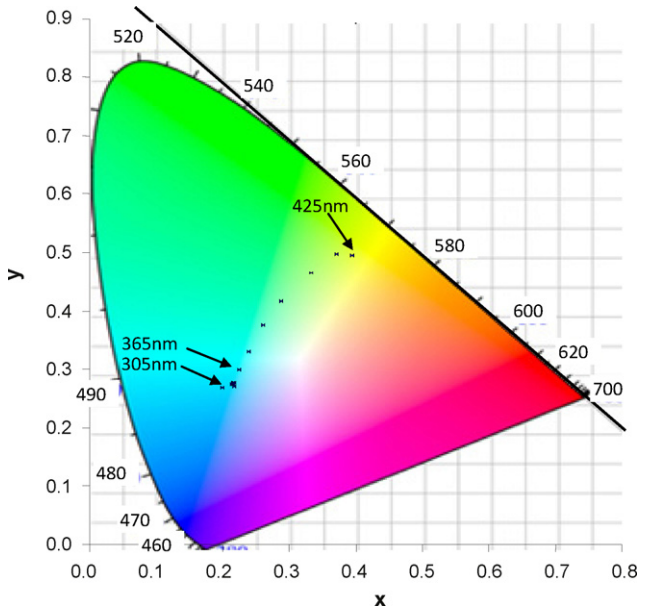

Fig. 2. CIE 1931 color diagram for excitation wavelengths from 305 to 425 nm with 10 nm steps.

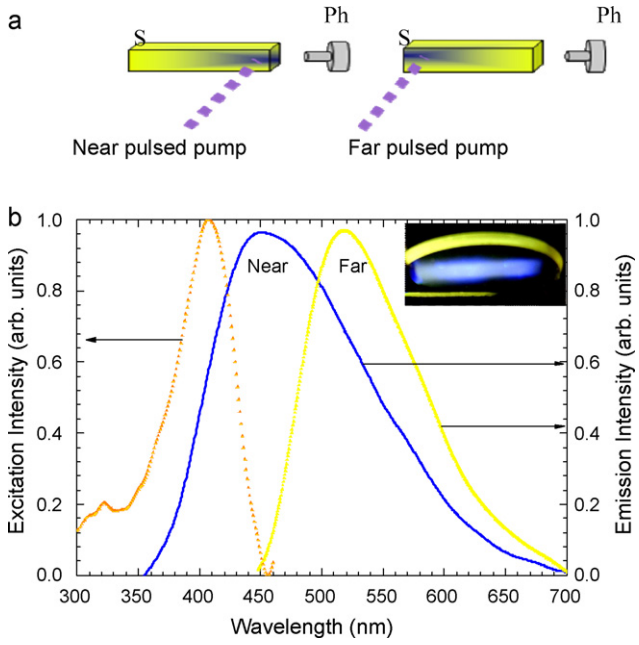

Fig. 3. (a) Scheme of the excitation near and far from the photodetector (Ph) in the Ce^{3+}:LSCAS glass under 355 nm excitation. The letter S is used to indicate the sample. (b) Emission spectra of the sample recorded in two different positions. The blue line is the emission spectrum observed under UV excitation and recorded near the excitation incidence. Orange dots represent the excitation band responsible for the yellow emission. The yellow line is the emission recorded in the sample far from the excitation source. (For interpretation of the references to color in this figure legend, the reader is referred to the web version of the article.)

405 nm, used to excite the LSCAS:Ce^{3+} glass and for color compensation to produce white light as shown in Ref. [18], we obtained a position of (0.23, 0, 53) in (u', v') color diagram, a Duv value of 0.014 and a CCT of 7000 K.

Fig. 1(a) also shows an intersection of the 410 nm excitation band, responsible for the yellow emission, with the 475 nm emission band. This result suggests a possible re-absorption mechanism of the blue emission by the yellow excitation band. This effect can be verified by exciting the glass sample under 355 nm from a 3rd harmonic of a pulsed Nd:YAG laser and observing the luminescence near and far from the excitation position, as shown by the scheme in Fig. 3(a). Fig. 3(b) shows that, by detecting the emission near the laser incidence on the glass, a broad blue emission band (blue line) is obtained. However, when the detection is made on the opposite side of the bulk, allowing the blue emission to propagate inside the glass until it is collected by the optical fiber, a broad yellow emission similar to those obtained by exciting the glass at 410 nm was observed. This effect can also be viewed in the photo in Fig. 3(b). It should be noted that the glass presents blue emission and a border yellow emission, regarding the position used to obtain the excitation spectra. This blue emission observed under 355 nm UV excitation, in the thermal range from 297 to 573 K, shows an exponential decrease behavior of its intensity with the temperature. This occurred due to the natural thermal quenching process without changing the wavelength of peak. This behavior indicates that we can neglect other possible energy sharing mechanisms between the two main sites, such as direct electronic transfer activated by thermal energy.

Table 1
Comparison of the luminescence peak position and band-width values for some Ce^{3+}-doped materials and the Ce^{3+}:LSCAS glass.

Material	Luminescence peak position (cm^{-1})	Band-width (cm^{-1})	Reference
Ce^{3+}:LSCAS	18,519	4583	This work
Ce^{3+}:LuAG	18,292	4086	[12]
Ce^{3+}/Li^{+}:Sr_3SiO_5	18,975	3472	[27]
Ce^{3+}:YAG	18,083	2995	[29]
Ce^{3+}:TAG	17,944	2752	[10]

The re-absorption mechanism indicates that there is another route to obtain tunable emission light by exciting the glass in the UV and by changing the thickness of the sample. Fig. 4 shows the position in the CIE 1931 color diagram of the broad emission bands obtained recording the emission for each 1 mm of translation of the laser incidence along the sample. In this figure, the zero point indicates that the detection is near the excitation point. The

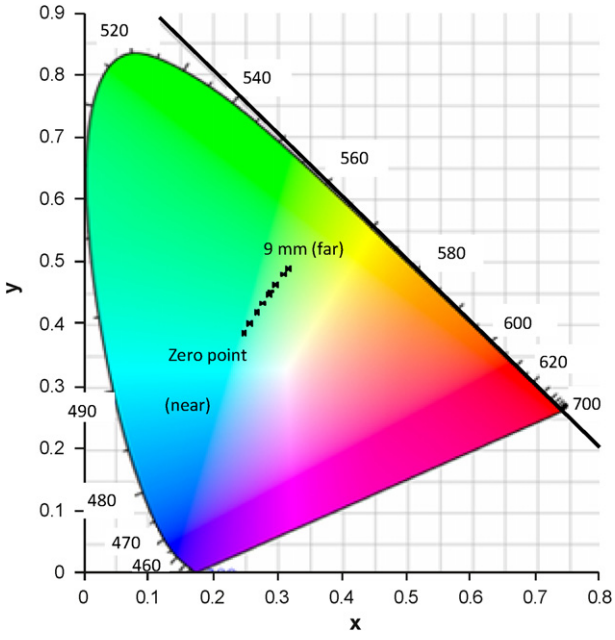

Fig. 4. CIE 1931 color diagram for UV excitation observing the emission in the sample at different positions with a 1 mm displacement step from the excitation position.

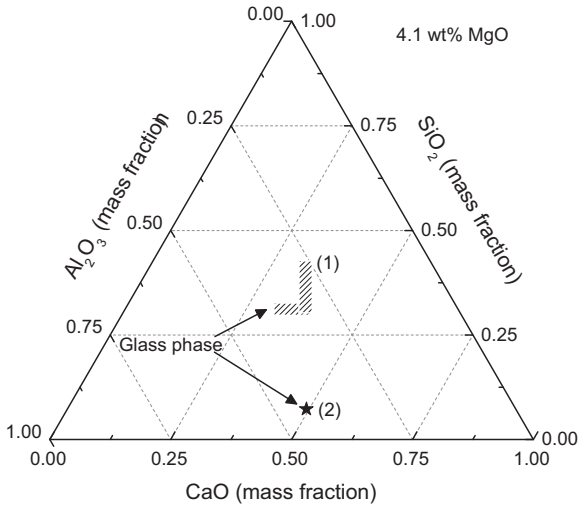

Fig. 5. Phase diagram of the $CaO/Al_2O_3/SiO_2$/4.1-wt.%–MgO system. There are two regions in which it is possible to obtain a glass phase with this chemical composition, which are labeled (1) and (2) and represent calcium-aluminosilicate (CAS) and low-silica-calcium-aluminosilicate (LSCAS) glasses, respectively.

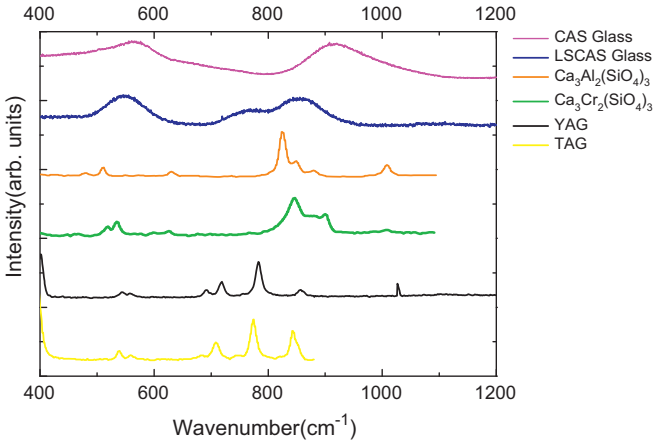

Fig. 6. Raman spectra for different silicate and aluminate garnet crystals and the CAS and LSCAS glasses.

position (x, y) in the CIE 1931 color diagram changes continuously from (0.25, 0.38) to (0.32, 0.49) and the relative color temperature ranges from 9088 to 5838 K for the near and far positions used to perform the excitation, respectively.

An important parameter for the use of a proposed material in WL applications is its color-rendering-index (CRI). This index is the unique internationally agreed metric for color-rendering evaluation. This index indicates the ability of a light source to reproduce the color of various objects faithfully in comparison with an ideal or natural light source [24]. For all emission spectra represented in the CIE color diagram in Fig. 4, the CRI values ranged from 59 to 75 for lower color temperatures (below 5000 K), obtained by exciting the sample from 380 to 425 nm, respectively. Despite the fact that the CRI values are lower than those of tetrachromatic WLEDs, it is important to mention that they were obtained without accounting for the blue-light compensation to produce WL. In the case of blue-light compensation, the expected CRI value for the Ce^{3+}:LSCAS glass should be higher than those for many well known WL materials, such as Ce^{3+}:Sr_3SiO_5 (CRI ~81) [25,26] or the classic Ce^{3+}:YAG (CRI ~ 70–80) [27,28]. This effect occurs because of the broader visible emission band of the Ce^{3+}:LSCAS glass, as previously discussed and summarized in Table 1.

These two ways of obtaining tunable light emission provide a singular characteristic of Ce^{3+}:LSCAS glass and represent a step towards solid-state smart white lighting when compared with traditional WLED materials, such as Ce^{3+}:YAG, whose luminescence has a fixed spectral position. Moreover, the use of just one phosphor ion, such as Ce^{3+}, is advantageous when compared with WL sources that use multiple emission phosphors to achieve one-color-tunable WL. In this case, each phosphor has a different degradation time, which results in an unexpected color shift over long use times [29]. In terms of the tunable light power, changing the excitation wavelength shows the widest coverage of the correlated color temperature, as can observed by comparing the emission positions in the CIE 1931 color diagrams, shown in Figs. 2 and 4.

3.2. Similarity of LSCAS glass structure with a disordered garnet one

The glass melting under vacuum conditions around 1600 °C using different Al_2O_3, CaO and SiO_2 contents has been described elsewhere [14]. Fig. 5 shows the phase diagram for different chemical compositions of calcium aluminosilicate glasses. There are two possible regions in which it is possible to obtain a glass phase, which are labeled (1) and (2). Region (1) shows glasses formed by a chemical composition of high silica content, which are called calcium-aluminosilicate glasses (CAS). In this case, glasses doped with cerium showed blue emission spectra (data not shown) similar to those of previously reported aluminosilicate glasses [30]. Our low-silica-content glass is located in the small glassy region, region (2), which is surrounded by a non-glass phase. This difference between CAS and LSCAS glasses leads to different optical and structural properties that can be observed by Raman spectra and measurements of the optical basicity and band gap, as previously reported [31].

The observed yellow emission of Ce^{3+}:LSCAS glass under violet excitation and the knowledge that this emission is only observed in materials with garnet structures led us to suppose that the LSCAS local glass structure may have similarities to the garnet structure. Consequently, the observed yellow emission is an indication that some Ce^{3+} ions in this glass are located in a non-ordered distribution of dodecahedral sites. These sites can be represented by distorted cubes with similar diameters. In this case, Ce^{3+} should be submitted to a strong pressure along one axis, resulting in an approximately tetragonal field similar to a rare-earth site [32]. This hypothesis can be verified by comparing the structure of the LSCAS glass with known garnet materials by Raman scattering spectroscopy. This procedure has been used in many works as a routine tool to characterize garnet structures. For glass materials, Raman spectroscopy is also an important tool that yields information on the number of bridging oxygen's per cation tetrahedron in the glass and on the non-bridging oxygen (NBO) content [14].

Fig. 6 shows the Raman spectra of different silicate and aluminate garnets crystals and CAS and LSCAS glasses that have high and low silica content, respectively. The Raman spectra of garnets are usually divided in two main vibrational regions: external and internal vibrations that are lower and higher than 400 cm^{-1}, respectively [33–35]. Because LSCAS and CAS glasses do not present any well defined Raman bands below 400 cm^{-1}, just a continuum non-zero signal shoulder, we will focus our discussion mainly on the region related to internal vibrations. Some examples of silicate garnets like grossular ($Ca_3Al_2(SiO_4)_3$) [31,33], uvarovite ($Ca_3Cr_2(SiO_4)_3$) [31,33] and aluminate garnets such as YAG [36] and TAG [37] present internal vibrations that can be divided in three main spectral regions: 450–550 cm^{-1}, 690–800 cm^{-1} and 800–910 cm^{-1}. These intervals are related to the internal vibrations of AlO_4 and SiO_4 tetrahedra present in the structure with similar energies. Some of these tetrahedra are inhomogeneously bound with neighbor atoms. As a

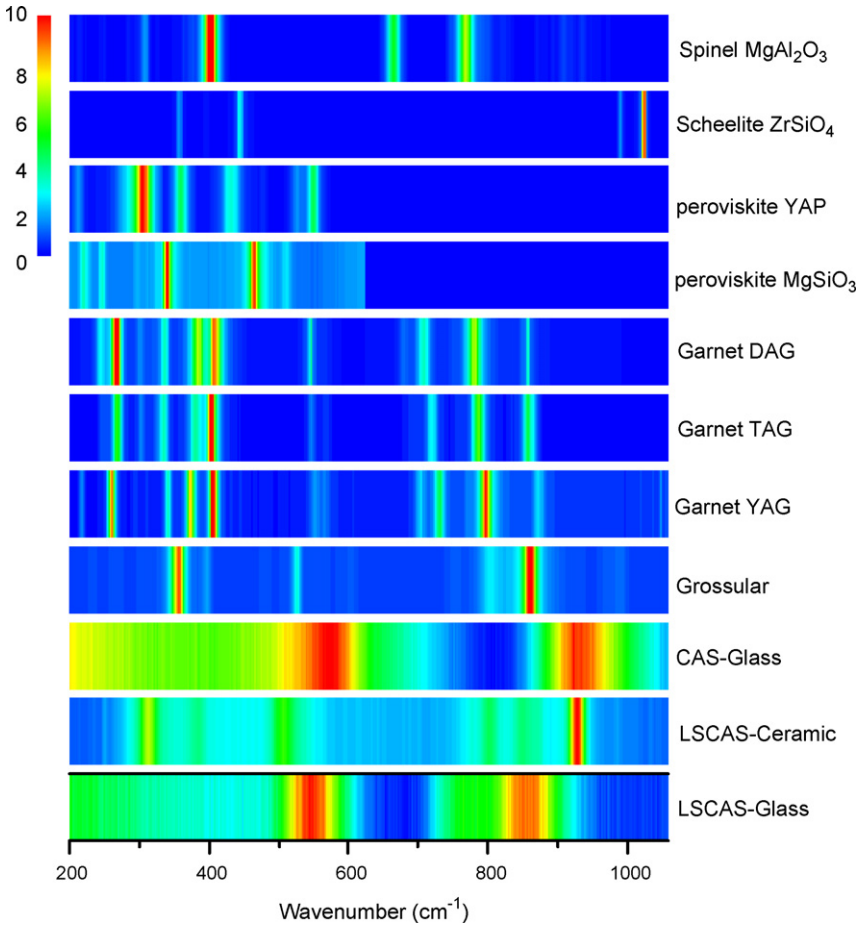

Fig. 7. Raman spectra in terms of peak intensities and positions of different aluminate and silicate garnets and non-garnet materials with chemical compositions containing Al_2O_3 and/or SiO_2, similar to the LSCAS-glass composition.

consequence of this influence of the surrounding, the vibrational energies change slightly, making the distinction between AlO_4 and SiO_4 tetrahedra very difficult. Concerning the Raman spectrum of LSCAS glass, it has a smaller ratio of SiO_2/AlO_2 compared with CAS and silicate garnets, and it is consequently expected that the contribution of AlO_4 tetrahedra vibrations in the Raman signal will be higher than those related to the SiO_4 vibrational modes. LSCAS glass presents a broad band centered at 550 cm^{-1}, which can be assigned to the $(Si–O)_{bend}$ and $(Al–O)_{bend}$ of SiO_4 and AlO_4 tetrahedra, respectively. The band at 790 cm^{-1} is evident in LSCAS glasses and not observed in CAS glasses or silicate garnets. For this reason, this band can be attributed to $(Al–O)_{stretch}$ of depolymerized Q^2 and Q^3 species of AlO_4 tetrahedra [29]. The notation Q^n, in which n is the number of bridging oxygen, is used to distinguish between the different tetrahedral species in the Raman results [38]. Between 800 and 1100 cm^{-1}, the Raman spectrum is characterized by the vibrational stretching of species containing NBOs. This spectral region is characterized by vibration modes related to $(Al, Si–O)_{strech}$ in tetrahedral groups with various number of NBO. Raman modes at approximately 1200, 1100, 950, 900, and 850 cm^{-1} have been associated with alumino or silicate tetrahedra in Q^4, Q^3, Q^2, Q^1, and Q^0 species, respectively [14]. Both aluminate and silicate garnets show Raman bands in this region. However, silicate garnets like uvarovite and grossular present vibrational bands slight displaced towards higher energy when compared with aluminate garnets like YAG and TAG. This result indicates that both silicate and aluminate garnets are similar in the spectral region related to internal vibrations.

The likeness discussed above can be more clearly observed by comparing the Raman spectra of different garnets and non garnet crystals with LSCAS glass. Fig. 7 shows the Raman spectra in terms of the peak intensities and positions of different aluminate and silicate garnets, such as $Ca_3Al_2(SiO_4)_3$ (grossular) [31,33], YAG [34], TAG and DAG [35], our LSCAS glass, and other non-silicate or -aluminate garnets such as $MgSiO_3$ [39], YAP [40], $ZrSiO_4$ [41] and $MgAl_2O_3$ [42]. Between 500 and 600 cm^{-1}, all aluminate- and silicate-garnet materials show vibration bands related to the Si, Al–O bands of tetrahedra, as previously mentioned, and bands between 700 and 950 cm^{-1} related to Si and Al–O stretch modes. This pattern is not observed in other materials with chemical compositions similar to the garnets or LSCAS glass that present the same vibrational bands in this region. Therefore, few similarities can be observed when these garnets are compared with other structures like perovskite and spinel.

Performing a thermal annealing over the crystallization temperature, the glass becomes ceramic without transparency. The Raman spectrum of this LSCAS ceramic shows bands located at 500, 800, 850 and 925 cm^{-1} (Fig. 7), which are narrower than those of LSCAS glass due to its more ordered structure. Except for the last one, all of the bands are located in the same spectral region of garnet materials. All of these bands are covered by the LSCAS glass Raman band. The 925-cm^{-1} band of LSCAS ceramic is located at the same position as that observed in the CAS glass. This result indicates that the LSCAS glass has a similar structure to garnet crystals in terms of the crystal field and symmetry of some sites. This similarity is also sustained by the yellow emission observed under violet excitation, which was only observed in Ce^{3+}-doped garnet materials until recently. The blue emission observed in Ce^{3+}-doped LSCAS under 350 nm excitation also indicates that

LSCAS presents some non garnet sites that are responsible for the blue emission observed in this glass. In summary, LSCAS presents two main structural phases related to a garnet and a non garnet ones. This non homogeneous characteristic is responsible for the two broad excitation bands located in the violet and ultraviolet regions and for the two broad emission bands observed in the visible region, useful for WLEDs with different color-temperature tunabilities.

4. Conclusions

The spectroscopic results of the Ce^{3+}:LSCAS glass indicate that it is a strong candidate for tunable light sources from the blue to yellow region with high CRI (~75%). The possibility of tuning the light by changing the excitation wavelength or adjusting the thickness of the sample confer to this glass a flexibility to obtain different emission wavelengths. This phenomenon is important in controlling the circadian response and visual comfort, which have not been taken into account in the research of new phosphors and deserve much more consideration. The reason for this ability is attributed to the structural characteristics of this glass that has different sites; some of them have a characteristic garnet structure represented by distorted cubes with similar diameters. These sites induce a strong pressure along one axis, resulting in an approximately tetragonal field similar to that of a rare-earth site. However, some other sites induce a weaker interaction that results in a blue emission under UV excitation. The broad band, which is a natural characteristic of rare-earth or transition-metal-doped glasses, improves the ability to change the color temperature. Thus, the technological challenges in the development of new WL devices, the ability to produce a sunlight-style emission with daylight chromaticity and a wide color-temperature span, which are associated with the regulation of circadian rhythm in humans, may achieved with this glass, as suggested by the results presented in this work.

Acknowledgments

The authors thank CAPES/COFECUB (Brazil/France cooperation) nº 565/07, CNPq, Fundação Araucária, and CNRS-UCBLyon1 for financial support of this work.

References

[1] S. Ye, F. Xiao, Y.X. Pan, Y.Y. Ma, Q.Y. Zhang, Mater. Sci. Eng. Rep. 71 (2010) 1–34.
[2] D. Zhao, S.-J. Seo, B.-S. Bae, Adv. Mater. 19 (2007) 3473–3479.
[3] Y. Chen, K.W. Cheah, M. Gong, J. Lumin. 131 (2011) 1589–1593.
[4] Z. Cui, R. Ye, D. Deng, Y. Hua, S. Zhao, G. Jia, C. Li, S. Xu, J. Alloys Compd. 509 (2011) 3553–3558.
[5] Y.Q. Li, J.E.J. van Steen, J.W.H. van Krevel, G. Botty, A.C.A. Delsing, F.J. DiSalvo, G. De With, H.T. Hintzen, J. Alloys Compd. 417 (2006) 273.
[6] Y.-C. Li, Y.-H. Chang, Y.-F. Lin, Y.-S. Chang, Y.-J. Lin, J. Alloys Compd. 439 (2007) 367–375.
[7] H. Yu, Y. Lai, G. Gao, L. Kong, G. Li, S. Gan, G. Hong, J. Alloys Compd. 509 (2011) 6635–6639.
[8] W.M. Yen, M. Raukas, S.A. Basun, W. van Schaik, U. Happek, J. Lumin. 69 (1996) 287–294.
[9] H.S. Jang, W.B. Im, D.C. Lee, D.Y. Jeon, S.S. Kim, J. Lumin. 126 (2007) 371–377.
[10] G. Blasse, A. Brill, J. Chem. Phys. 47 (1967) 5139–5145.
[11] J. Bei, G. Qian, X. Liang, S. Yuan, Y. Yang, G. Chen, Mater. Res. Bull. 42 (2007) 1195–1200.
[12] M. Batentschuk, A. Osvet, G. Schierning, A. Klier, J. Schneider, A. Winnacker, Radiat. Meas. 38 (2004) 539–543.
[13] A.A. Setlur, A.M. Srivastava, Opt. Mater. 29 (2007) 1647–1652.
[14] A. Steimacher, N.G.C. Astrath, A. Novatski, F. Pedrochi, A.C. Bento, M.L. Baesso, A.N. Medina, J. Non-Cryst. Solids 352 (2006) 3613–3617.
[15] D.F. de Sousa, J.A. Sampaio, L.A.O. Nunes, M.L. Baesso, A.C. Bento, L.C.M. Miranda, Phys. Rev. B 62 (2000) 3176–3180.
[16] D.F. de Sousa, L.A.O. Nunes, J.H. Rohling, M.L. Baesso, Appl. Phys. B 77 (2003) 59–63.
[17] Y. Guyot, A. Steimacher, M.P. Belançon, A.N. Medina, M.L. Baesso, S.M. Lima, L.H.C. Andrade, A. Brenier, A.M. Jurdyc, G. Boulon, Spectroscopic properties, concentration quenching and laser investigations of Yb^{3+}-doped calcium aluminosilicate glasses. J. Opt. Soc. Am. B, in press.
[18] L.H.C. Andrade, S.M. Lima, A. Novatski, P.T. Udo, N.G.C. Astrath, A.N. Medina, A.C. Bento, M.L. Baesso, Y. Guyot, G. Boulon, Phys. Rev. Lett. 100 (2008) 027402.
[19] S.M. Lima, J.R. Silva, L.H.C. Andrade, A. Novatski, A.N. Medina, A.C. Bento, M.L. Baesso, Y. Guyot, G. Boulon, Opt. Lett. 35 (2010) 1055–1057.
[20] L.H.C. Andrade, S.M. Lima, A. Novatski, A. Steimacher, J.H. Rohling, A.N. Medina, A.C. Bento, M.L. Baesso, Y. Guyot, G. Boulon, Appl. Phys. Lett. 95 (2009) 081104–081106.
[21] J.A. Sampaio, T. catunda, F.C.G. Gandra, S. Gama, A.C. Bento, L.C.M. Miranda, M.L. Baesso, J. Non-Cryst. Solids 247 (1999) 196–202.
[22] M.L. Baesso, A.C. Bento, A.R. Duarte, A.M. Neto, L.C.M. Miranda, J.A. Sampaio, T. Catunda, S. Gama, F.C.G. Gandra, J. Appl. Phys. 85 (1999) 8112–8118.
[23] A.A. Setlur, W.J. Heward, Y. Gao, A.M. Srivastava, R.G. Chandran, M.V. Shankar, Chem. Mater. 18 (2006) 3314–3322.
[24] Z. Lei, G. Xia, L. Ting, G. Xiaoling, L.Q. Ming, S. Guangdi, Microeletron. J. 38 (2007) 1–6.
[25] H.S. Jang, D.Y. Jeon, Opt. Lett. 32 (2007) 3444–3446.
[26] H.S. Jang, D.Y. Jeon, Appl. Phys. Lett. 90 (2007) 041906.
[27] A.A. Setlur, Electrochem. Soc. Interface 18 (2009) 32–36.
[28] Y. Pan, M. Wu, Q. Su, J. Phys. Chem. Solids 65 (2004) 845–850.
[29] E.F. Schubert, J.K. Kim, Science 308 (2005) 1274–1278.
[30] B. Wang, L. Sun, H. Ju, Solid State Commun. 150 (2010) 1460–1462.
[31] A. Novatski, A. Steimacher, A.N. Medina, A.C. Bento, M.L. Baesso, L.H.C. Andrade, S.M. Lima, Y. Guyot, G. Boulon, J. Appl. Phys. 104 (2008) 094910.
[32] J.L. Wu, G. Gundiah, A.K. Cheetham, Chem. Phys. Lett. 441 (2007) 250–254.
[33] B.A. Kolesov, C.A. Geiger, Phys. Chem. Miner. 25 (1998) 142–151.
[34] R.K. Moore, W.B. White, T.V. Long, Am. Mineral. 56 (1971) 54–71.
[35] D. Bersani, S. Ando, P. Vignola, G. Moltifiori, I.G. Marino, P.P. Lottici, V. Diella, Spectrochim. Acta A 73 (2009) 484–491.
[36] D.-L. Sun, Q.-L. Zhang, S.-M. Wan, H.-H. Jiang, S.-T. Yin, Optoelectron. Lett. 3 (2007) 0441–0443.
[37] K. Papagelis, J. Arvanitidis, G. Kanellis, S. Ves, G.A. Kourouklis, Physica B 265 (1999) 277–281.
[38] L. Cormier, D. Ghaleb, D.R. Neuville, J.M. Delaye, G. Calas, J. Non-Cryst. Solids 332 (2003) 255–270.
[39] D.J. Durben, G.H. Wolf, Am. Mineral. 77 (1992) 890–893.
[40] J.J. Romero, E. Montoya, L.E. Bausa, F.A. Rueda, M.R.B. Andreeta, A.C. Hernandes, Opt. Mater. 24 (2004) 643–650.
[41] M. Lang, F. Zhang, J. Lian, C. Trautmann, R. Neumann, R.C. Ewing, Earth Planet. Sci. Lett. 269 (2008) 291–295.
[42] D. Simeone, C. Dodane-Thiriet, D. Gosset, P. Daniel, M. Beauvy, J. Nucl. Mater. 300 (2002) 151–160.